Deciphering mesenchymal drivers of human Dupuytren's disease at single-cell level

Deciphering Mesenchymal Drivers of Human Dupuytren's Disease at Single-Cell Level

JID Open

Ross Dobie[1,5], Chris C. West[1,2,3,5], Beth E.P. Henderson[1,5], John R. Wilson-Kanamori[1], Dyana Markose[1], Laura J. Kitto[1], Jordan R. Portman[1], Mariana Beltran[1], Sadaf Sohrabi[1], Ahsan R. Akram[1], Prakash Ramachandran[1], Li Yenn Yong[2], Dominique Davidson[2] and Neil C. Henderson[1,4]

Dupuytren's disease (DD) is a common, progressive fibroproliferative disease affecting the palmar fascia of the hands, causing fingers to irreversibly flex toward the palm with significant loss of function. Surgical treatments are limited; therefore, effective new therapies for DD are urgently required. To identify the key cellular and molecular pathways driving DD, we employed single-cell RNA sequencing, profiling the transcriptomes of 35,250 human single cells from DD, nonpathogenic fascia, and healthy dermis. We identify a DD-specific population of pathogenic PDPN$^+$/FAP$^+$ mesenchymal cells displaying an elevated expression of fibrillar collagens and profibrogenic genes. In silico trajectory analysis reveals resident fibroblasts to be the source of this pathogenic population. To resolve the processes governing DD progression, genes differentially expressed during fibroblast differentiation were identified, including upregulated *TNFRSF12A* and transcription factor *SCX*. Knockdown of *SCX* and blockade of TNFRSF12A inhibited the proliferation and altered the profibrotic gene expression of cultured human FAP$^+$ mesenchymal cells, demonstrating a functional role for these genes in DD. The power of single-cell RNA sequencing is utilized to identify the major pathogenic mesenchymal subpopulations driving DD and the key molecular pathways regulating the DD-specific myofibroblast phenotype. Using this precision medicine approach, inhibition of TNFRSF12A has shown potential clinical utility in the treatment of DD.

Journal of Investigative Dermatology (2022) **142,** 114–123; doi:10.1016/j.jid.2021.05.030

INTRODUCTION

Dupuytren's disease (DD) is a common, progressive fibroproliferative disease affecting the palmar fascia of the hands. Contracture of this diseased fascia causes the fingers to irreversibly flex toward the palm, with significant loss of function and psychological morbidity (Wilburn et al., 2013). Surgery remains the preferred treatment for many patients with DD; however, even after effective surgery, patients may be left with permanent dysfunction owing to established joint contractures and recurrence rates are high (van Rijssen et al., 2012). Given the limitations of surgical treatment, effective new therapies for patients with DD are urgently required.

The mesenchyme is the major source of pathological matrix deposition during fibrosis (Henderson et al., 2020; Hinz et al., 2007). Accurate identification and targeting of specific subpopulations of mesenchymal cells have significantly reduced fibrosis in animal models of fibrotic disease, including skin fibrosis (Dulauroy et al., 2012; Jiang et al., 2018). Given that no animal models faithfully replicate DD, a similar animal model–based approach is not possible; therefore, we procured fresh DD tissue and used single-cell RNA sequencing (scRNA-seq) to interrogate the key cellular and molecular mechanisms regulating DD.

Recent studies using scRNA-seq have greatly advanced our understanding of mesenchymal cell functional heterogeneity during fibrosis (Croft et al., 2019; Dobie et al., 2019; Guerrero-Juarez et al., 2019; Kuppe et al., 2021; Ramachandran et al., 2019). To interrogate the key pathogenic mesenchymal cell subpopulations driving DD, we profiled the transcriptomes of 35,250 single cells from DD tissue, healthy dermis, and nonpathogenic (Skoog's) fascia. Our data (i) describe a single-cell atlas of the healthy dermis and fascia and DD tissue, (ii) characterize both transcriptionally and spatially the mesenchymal cellular compartment in DD, (iii) uncover a population of pathogenic PDPN$^+$ myofibroblasts (Myofibs) that likely originate from resident fibroblasts (FBs), (iv) resolve the key molecular mechanisms driving the PDPN$^+$ Myofib phenotype, and (v) identifies TNFRSF12A expressed on pathogenic

[1]*Centre for Inflammation Research, The Queen's Medical Research Institute, Edinburgh BioQuarter, The University of Edinburgh, Edinburgh, United Kingdom;* [2]*Department of Plastic, Reconstructive and Burns Surgery, St John's Hospital, Livingston, United Kingdom;* [3]*Department of Plastic, Reconstructive and Hand Surgery, Leeds General Infirmary, Leeds, United Kingdom; and* [4]*MRC Human Genetics Unit, Institute of Genetics and Cancer, The University of Edinburgh, Edinburgh, United Kingdom*

[5]*These authors contributed equally to this work.*

Correspondence: Neil C. Henderson, Centre for Inflammation Research, The Queen's Medical Research Institute, Edinburgh BioQuarter, The University of Edinburgh, Edinburgh, United Kingdom, EH16 4TJ. E-mail: Neil.Henderson@ed.ac.uk

Abbreviations: DD, Dupuytren's disease; EdU, 5-ethynyl-2′-deoxyuridine; FB, fibroblast; Myofib, myofibroblast; scRNA-seq, single-cell RNA sequencing; siRNA, small interfering RNA

Received 1 March 2021; revised 24 May 2021; accepted 25 May 2021; accepted manuscript published online 16 July 2021; corrected proof published online 4 November 2021

PDPN$^+$ Myofibs as a therapeutic target to treat patients with DD.

RESULTS

A single-cell atlas of the human dermis and fascia in health and in DD

Single, live cells were isolated from DD tissue, nonpathogenic fascia (from the transverse ligament of the palmar aponeurosis, referred to as Skoog's fascia in this paper), and healthy dermis. All tissues were taken at the time of corrective surgery for DD. scRNA-seq and unbiased clustering of 35,250 cells from nine samples (n = 3 DD, n = 3 Skoog's fascia, and n = 3 healthy dermis) revealed 18 distinct populations (Figure 1a and b and Supplementary Figure S1a). Annotation of cell lineages showed the successful isolation of all major cell types across the nine samples (Figure 1c and Supplementary Figure S1b and c and Supplementary Table S1). Quality control metrics were comparable across lineages (Supplementary Figure S1d). Subpopulation markers were identified across all clusters and lineages (Figure 1d and Supplementary Table S2).

To resolve the cellular landscape of DD, we performed immunofluorescence staining using lineage markers identified from the scRNA-seq analysis (Supplementary Figure S2a). CD68$^+$ mononuclear phagocytes and PECAM1$^+$ endothelia were located throughout the DD fibrotic niche, but PDGFRB$^+$ mesenchymal cells represented the most abundant cell type (Figure 1e). Mesenchymal cells were the predominant expressers of fibrillar collagens (types I and III) (Supplementary Figure S2b).

Identifying the pathogenic mesenchymal subpopulation in DD

To further interrogate mesenchymal cell functional heterogeneity and identify the profibrotic mesenchymal cell subpopulations driving DD, we reclustered the mesenchymal cells identifying four distinct clusters (Figure 2a). Whereas clusters 1–3 were populated by cells from all the three of the sampled areas, cluster 4 almost exclusively contained cells isolated from DD tissue (Figure 2b and c and Supplementary Figure S3a).

Differentially expressed marker gene analysis (Figure 2d and e and Supplementary Table S3) combined with immunofluorescence staining (Figure 2f) allowed annotation of the topography of these mesenchymal subpopulations. The mesenchymal subpopulations within DD were identified as vascular smooth muscle cells (cluster 1), pericytes (cluster 2), FBs (cluster 3), and Myofibs (cluster 4). PDPN$^+$ Myofibs represented the predominant mesenchymal population within the fibrotic region of DD but were not observed in nonpathogenic Skoog's fascia (Figure 2f and Supplementary Figure S3b). Expression of a Myofib signature, based on fibrillar collagens (*COL1A1*, *COL1A2*, *COL3A1*) and *ACTA2*, was highest in cluster 4 (Supplementary Figure S3c and d). Each subpopulation was functionally profiled using Gene Ontology analysis (Supplementary Table S3), with the derived terms matching known functions for each mesenchymal cell type (Figure 2g). Those associated with the Myofib cluster included collagen fibril organization, extracellular matrix organization, response to wounding, and other terms highly relevant to the known scar-forming role of Myofibs.

PDPN$^+$ Myofibs expressed the unique marker *FAP* (Supplementary Figure S3e and Supplementary Table S3), allowing FACS-based isolation of these cells from DD tissue (Supplementary Figure S3f). Immunostaining confirmed colocalization of FAP and PDPN$^+$ Myofibs in DD (Supplementary Figure S3g).

To assess whether further heterogeneity exists in the FB population, we performed further unbiased clustering of the subsetted mesenchymal cells at a higher resolution, identifying seven clusters with varying contributions from each of the sampled areas (Supplementary Figure S4). We annotated the clusters as vascular smooth muscle cells (cluster 1), pericytes (cluster 6), Myofibs (cluster 3), and FBs (FB1–4; clusters 2, 4, 5, and 7) (Supplementary Figure S4). FBs from DD tissue have previously been shown to divide into three major subsets annotated as PDPN$^+$, CD34$^+$, and ICAM1$^+$ (IL6^{low} and IL6^{high}) FBs (Layton et al., 2020). By creating a signature based on the top differentially expressed genes in these populations, we identified a high degree of transcriptional congruency between the FB populations identified in both studies (Supplementary Figure S4c).

Origin of PDPN$^+$ Myofibs in DD

To assess the origin of PDPN$^+$ Myofibs in DD, we performed in silico trajectory analyses on the mesenchymal cell dataset. Interrogation of cellular dynamics by unspliced and spliced mRNA ratios (scVelo) (Bergen et al., 2020) and pseudotemporal trajectory (Slingshot) (Street et al., 2018) uncovered potential differentiation from resident PDGFRA$^+$ FBs into the pathogenic PDPN$^+$ Myofib population, with no equivalent dynamics observed from vascular smooth muscle cells or pericytes to PDPN$^+$ Myofibs (Figure 3a). Additional RNA velocity analyses demonstrated an upregulation (positive velocity) of the fibrillar collagens in the PDPN$^+$ Myofib population (Supplementary Figure S5a).

Performing differential gene analysis along the differentiation trajectory, we defined five modules of coexpressed genes, with the first three modules representing genes downregulated with varying dynamics along the trajectory and the remaining two representing those upregulated during FB activation (Figure 3c and d and Supplementary Figure S5b and Supplementary Table S4). Modules 4 and 5 contained multiple profibrogenic genes, including *COL1A1*, *COL1A2*, *COL3A1*, *MMP2*, *TIMP2*, and *ITGAV* (Arpino et al., 2015; Henderson et al., 2013; Murray et al., 2017), and displayed Gene Ontology terms consistent with fibrogenesis (Figure 3d and Supplementary Table S4).

A similar differentiation trajectory from resident PDGFRA$^+$ FBs into the pathogenic PDPN$^+$ Myofibs and the associated upregulation of profibrotic genes were observed when performing the same trajectory analysis using only cells isolated from DD tissue (Supplementary Figure S5c–f and Supplementary Table S4). These data suggest that the PDPN$^+$ pathogenic Myofib subpopulation in DD originates from a resident PDGFRA$^+$ fascial FB population.

To gain insight into the transcriptional regulation of the FB to Myofib transition and of the Myofib phenotype in DD,

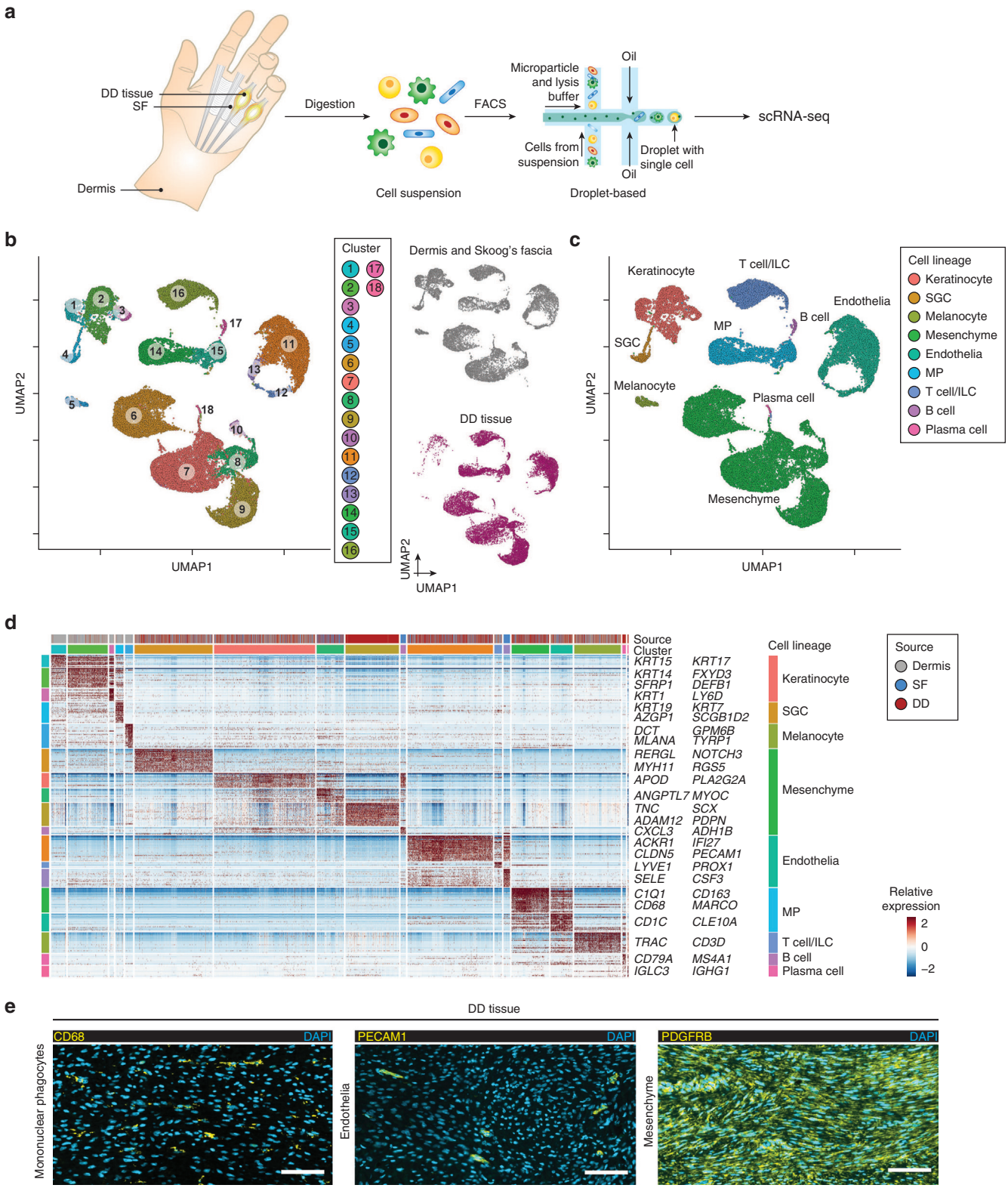

Figure 1. Resolving the cellular landscape of DD tissue. (**a**) Overview illustrating the scRNA-seq pipeline for cells from the dermis, SF, and DD tissue. (**b**) UMAP visualization of the clustering 35,250 cells from dermis (n = 3), SF (n = 3), and DD tissue (n = 3). Right shows the annotation by condition. SF and dermis represent nonpathogenic control tissue. (**c**) UMAP visualization of cell lineage inferred from the expression of marker gene signatures. (**d**) Heatmap of cluster marker genes (top shows the color coded by source and cluster), with cell lineage and exemplar genes labeled (right). Columns denote cells; rows denote genes. (**e**) Representative immunofluorescence images of identified lineages markers in DD tissue (fibrotic region). Left: CD68 (yellow) and DAPI (blue); middle: PECAM1 (yellow) and DAPI (blue); right: PDGFRB (yellow) and DAPI (blue). Bar = 100 μm. DD, Dupuytren's disease; ILC, innate lymphoid cell; K, keratin; MP, mononuclear phagocyte; scRNA-seq, single-cell RNA sequencing; SF, Skoog's fascia; SGC, sweat gland cell; UMAP, uniform manifold approximation and projection.

we cross-referenced our gene set from the FB differentiation trajectory (Figure 3 and Supplementary Table S4) with a curated list of human transcription factors (Lambert et al., 2018). This identified 20 transcription factors with altered expression along the FB differentiation trajectory, six of which were upregulated—*SOX4*, *FOXP1*, *AEBP1*, *MAFB*, *DMRT2*, *SCX* (Figure 3e and Supplementary Table S4).

Of the six identified transcription factors that were upregulated along the differentiation trajectory, *SCX* and *DMRT2* showed the highest specificity to the profibrotic PDPN$^+$ Myofib population (Figure 3f and g). SCX, a basic helix-loop-helix transcription factor, is highly expressed in extracellular matrix–rich tissues, including fibrotic human lung, and has previously been shown to play an important role in regulating FB and Myofib phenotype (Bagchi et al., 2016; Espira et al., 2009; Ramírez-Aragón et al., 2020). To interrogate whether *SCX* regulates the Myofib phenotype in DD, we performed small interfering RNA (siRNA)-mediated knockdown of *SCX* in primary FAP$^+$ Myofibs isolated from DD tissue. *SCX* knockdown reduced the expression of *COL1A2* and decreased the proliferation of Myofibs isolated from DD tissue (Figure 3h and i). These data indicate an important functional role for the transcription factor SCX in the regulation of the pathogenic DD Myofib phenotype.

Therapeutic targeting of PDPN$^+$ pathogenic Myofibs in DD

To facilitate the identification of potential antifibrotic pharmacological targets in DD, we used CellPhoneDB (Efremova et al., 2020) to refine the pseudotemporal gene coexpression modules 4 and 5, including only ligands and receptors. A total of 26 genes upregulated along the FB activation trajectory were uncovered (Figure 4a and Supplementary Figure S6a and Supplementary Table S4).

To facilitate precision targeting of the pathogenic mesenchymal subpopulation in DD, we assessed which of the 26 upregulated ligands and receptors identified along the Myofib differentiation trajectory were specific to the pathogenic Myofib population. Nine ligands and receptors showed high specificity to the pathogenic Myofib population, including *TNFRSF12A* (Figure 4b and Supplementary Figure S6b and c). Immunofluorescence staining confirmed the expression of TNFRSF12A on PDPN$^+$ pathogenic Myofibs in DD tissue (Figure 4c). In contrast, *TNFSF12* (the ligand for TNFRSF12A) was widely expressed in multiple cell lineages in our dataset (Supplementary Figure S6d).

TNFSF12 induced the proliferation and activation of primary FAP$^+$ Myofibs isolated from DD tissue ex vivo, and this was inhibitable by TNFRSF12A blockade (Figure 4d and e). These data show an important regulatory role for the TNFSF12–TNFRSF12A pathway in the expansion and activation of pathogenic Myofibs and identify a potential pharmacological target to treat patients with DD.

DISCUSSION

Single-cell genomics approaches are driving a step change in our ability to interrogate mesenchymal cell heterogeneity (Ascensión et al., 2021; He et al., 2020; Tabib et al., 2018; Vorstandlechner et al., 2020). The ability to precisely identify human disease–specific pathogenic subpopulations and to uncover the molecular mechanisms regulating these aberrant cell states has the potential to greatly accelerate the identification of relevant and tractable therapeutic targets (Dobie and Henderson, 2019; Henderson et al., 2020). In this study, we used scRNA-seq of DD tissue and control tissue (nonpathogenic fascia and dermis) to resolve the pathogenic mesenchymal subpopulations and molecular mechanisms driving DD.

Myofibs are the major source of extracellular matrix deposition during organ fibrosis and have garnered considerable attention as targets for therapeutic intervention (Yazdani et al., 2017). scRNA-seq of fibrotic human tissue has facilitated the in-depth characterization of the mesenchymal compartment in multiple fibrotic conditions, uncovering profibrogenic mechanisms driving Myofib phenotype (Kuppe et al., 2021; Ramachandran et al., 2019). Functionally distinct populations of mesenchymal cells exist in DD, with densely packed Myofibs representing a large component of the fibrotic niche (Layton et al., 2020; Verjee et al., 2013, 2009). In this study, we transcriptionally profiled the entire mesenchymal compartment in DD at the single-cell level. This allowed the identification of a disease-specific PDPN$^+$ Myofib population residing in the DD fibrotic niche, absent in nonpathogenic fascia or dermis. No animal models of DD exist, eliminating the possibility of performing formal genetic lineage-tracing experiments to assess DD Myofib origin. Nevertheless, our in silico trajectory analyses suggest that the PDPN$^+$ Myofib population observed in DD datasets arises from resident fascial PDGFRA$^+$ FBs, implying that a resident PDGFRA$^+$ FB–Myofib transition occurs in DD.

To functionally interrogate the molecular mechanisms regulating pathogenic Myofib phenotype in DD, we developed a protocol to isolate pathogenic PDPN$^+$/FAP$^+$ Myofibs from DD tissue for ex vivo analysis. Validating our scRNA-seq data, we showed that *SCX* plays an important role in the transcriptional regulation of DD Myofib phenotype, modulating *COL1A2* expression and cell proliferation. A similar role for *SCX* has previously been identified in cardiac Myofibs (Espira et al., 2009). Furthermore, we show that pharmacological blockade of TNFRSF12A inhibits DD Myofib expansion and activation. TNFSF12–TNFRSF12A signaling has previously been shown to have important regulatory roles in mesenchymal cell proliferation and activation in other fibrotic diseases (Gomez et al., 2016; Wilhelm et al., 2016).

This work highlights the power of single-cell transcriptomics to identify both the major pathogenic mesenchymal subpopulations driving DD and the key molecular pathways regulating Myofib phenotype during DD. Using this precision medicine approach, our findings suggest that inhibition of TNFRSF12A has clinical potential in the treatment of patients with DD.

MATERIALS AND METHODS

Tissue procurement

Human tissue was collected from patients undergoing elective surgical procedures with previous written informed consent. Permission for the collection, storage, and subsequent research was granted in

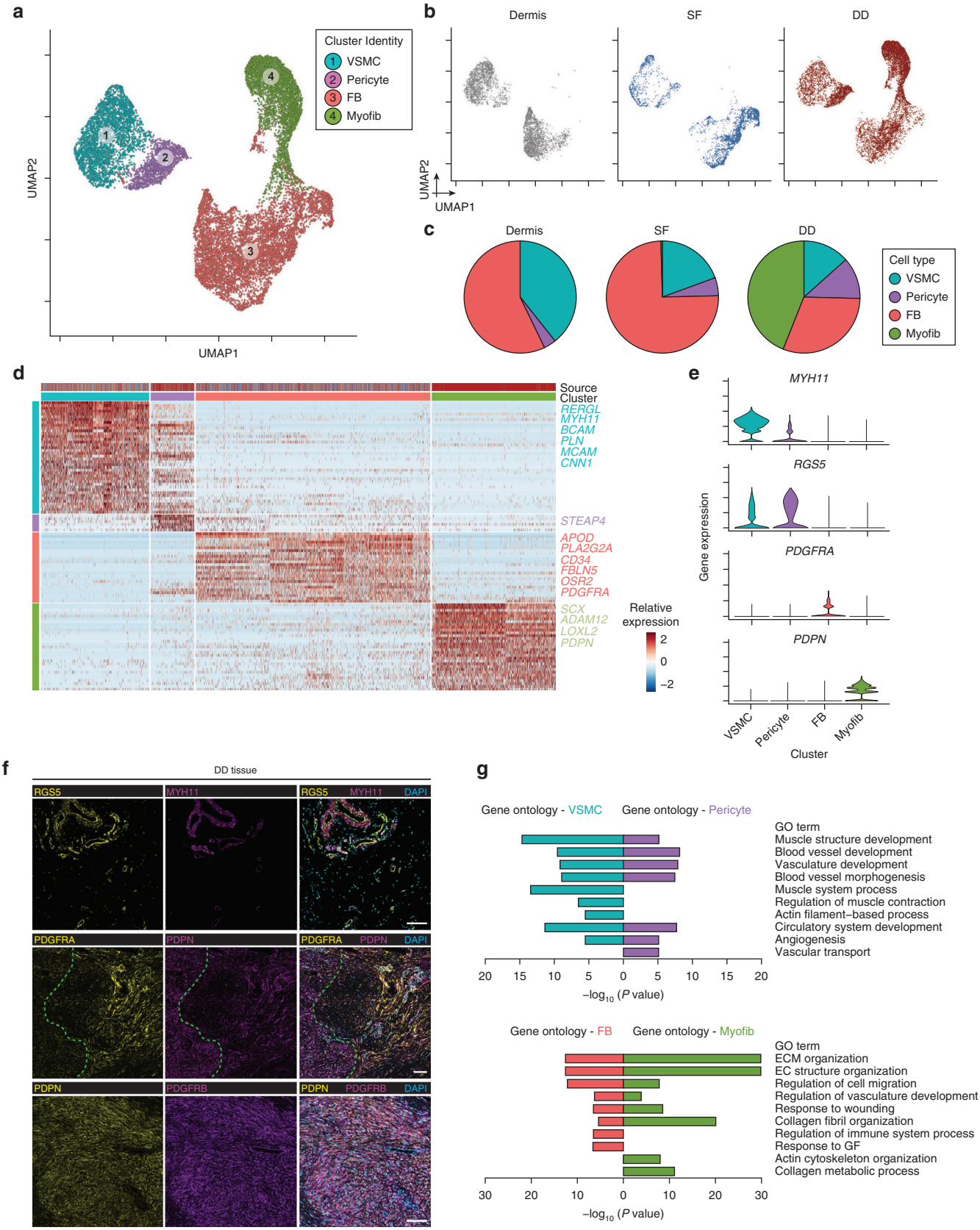

Figure 2. Identifying the pathogenic mesenchyme subpopulation in DD. (**a**) UMAP visualization of the clustering 16,988 mesenchymal cells from dermis (n = 3), SF (n = 3), and DD tissue (n = 3). (**b**) UMAP visualization of cells per source. (**c**) Pie charts of the proportion of clusters per source. (**d**) Heatmap of cluster marker genes (top shows the color coded by source and cluster), with exemplar genes labeled (right). Columns denote cells; rows denote genes. (**e**) Expression of selected marker genes across mesenchymal clusters. (**f**) Representative immunofluorescence images of identified markers in DD tissue. Top (nonfibrotic region) shows RGS5 (yellow), MYH11 (purple), and DAPI (blue); middle (edge of fibrotic region) shows PDGFRA (yellow), PDPN (purple), and DAPI (blue); bottom

Edinburgh by the South East Scotland Research Ethics Committee 01 (Ref: 16/SS/0103).

Tissue processing

For scRNA-seq and flow cytometry analysis, surgical tissue was immediately placed in media and transported directly to the laboratory, and dissociation routinely commenced within 90 minutes of surgical excision. For histological assessment, samples were fixed in 4% neutral-buffered formalin for 24 hours followed by paraffin embedding.

Preparation of single-cell suspensions

Before preparation of a single-cell suspension, epidermis and subcutaneous fat were removed from healthy skin using scissors. For scRNA-seq and cell sorting, samples were prepared as previously described (Ramachandran et al., 2019).

Cell sorting

Incubation with primary antibodies was performed for 20 minutes at 4 °C. All antibodies, conjugates, lot numbers, and dilutions used in this study are presented in Supplementary Table S5. After antibody staining, cells were washed with PEB buffer (PBS, 0.1% BSA and 2mM EDTA). For cell sorting (FACS), cell viability staining (DAPI; 1:1,000 dilution) was performed immediately before acquiring the samples.

Cell sorting for scRNA-seq and cell culture was performed on a BD FACSAria Fusion (BD, Franklin Lakes, NJ). For scRNA-seq, viable ($DAPI^-$) single cells were sorted and processed for droplet-based scRNA-seq. For culturing of primary Myofibs, viable single $CD45^-$/$CD144^-$/$EPCAM^-$/FAP^+ cells were sorted from DD tissue.

Cell culture

Primary human FAP^+ Myofibs were cultured using an FGM-2 Fibroblast Growth Medium-2 BulletKit culturing system containing basal medium (FB growth medium) and supplements (Lonza, Basel, Switzerland, CC-3132), according to the manufacturer's instructions. All experiments were performed using cells between passages 3 and 5.

For assessment of gene expression, Myofibs were plated at 100,000 cells per well in a 12-well plate (Corning Inc, Corning, NY, 3513). For the assessment of proliferation, Myofibs were plated at 10,000 cells per well in a 96-well plate (Corning, 3595). Before commencing knockdown or proliferation assays, Myofibs were serum starved overnight in a FB growth medium without supplements.

SCX knockdown in primary human DD Myofib

Knockdown of *SCX* in human Myofibs was performed using siRNA. siRNA duplexes with Lipofectamine RNAiMAX Transfection Reagent (Invitrogen/Thermo Fisher Scientific, Waltham, MA, 13778075) were prepared in Opti-MEM (Gibco/Thermo Fisher Scientific, 31985070) according to the manufacturer's instructions and were used at a concentration of 25 nM.

For assessment of gene expression, cells were exposed to the duplex for 48 hours in a FB growth medium containing all supplements except GA-1000. Cells were collected for RT-qPCR. Knockdown efficiency was assessed by *SCX* RT-qPCR. The best siRNA for knockdown was determined empirically using the FlexiTube GeneSolution kit (Qiagen, Hilden, Germany, GS642658). Myofibs treated with control siRNA (Qiagen, 1027280) and siRNA for *SCX* (Qiagen, Hs_LOC642658 4, SI02797634) were then assessed for fibrillar collagen and *ACTA2* gene expression.

For assessment of proliferation, cells were treated with control siRNA and siRNA for *SCX* for 24 hours in FB growth medium containing all supplements except GA-1000. The 5-ethynyl-2′-deoxyuridine (EdU) (100 μM) was added for the final 3 hours of culturing. Cells were then fixed in 4% neutral-buffered formalin for 10 minutes at 4 °C and then washed and stored (at 4 °C) in PBS.

TNFRSF12A inhibition in primary human DD Myofibs

For assessment of gene expression, primary FAP^+ Myofibs were treated with (1) TNFSF12 (100 ng/ml) with or without anti-TNFRSF12A (2 μg/ml) (Life Technologies, Carlsbad, CA, 16-9018-82, clone ITEM-4) or mouse IgG2b kappa isotype control antibody (2 μg/ml) (Life Technologies, 16-4732-82, clone eBMG2b), or (2) vehicle control as indicated for 48 hours. Cells were collected for qPCR with reverse transcription, that is, RT-qPCR.

For assessment of proliferation, Myofibs were treated with (1) TNFSF12 (100 ng/ml) with or without anti-TNFRSF12A (2 μg/ml) or mouse IgG2b kappa isotype control antibody (2 μg/ml), or (2) vehicle control as indicated for 24 hours. EdU 100 μM was added for the final 3 hours of culturing. Cells were then fixed in 4% neutral-buffered formalin for 10 minutes at 4 °C and then washed and stored (at 4 °C) in PBS.

RNA extraction and RT-qPCR

RNA was isolated from Myofibs using the RNeasy Plus Micro Kit (Qiagen, 74034), and cDNA synthesis was performed using the QuantiTect Reverse Transcription Kit (Qiagen, 205313) according to the manufacturer's instructions. Reactions were performed in 384-well plate format and were assembled using the QIAgility automated pipetting system (Qiagen). RT-qPCR was performed to assess *SCX* expression using TaqMan Fast Advanced Master Mix (Applied Biosystems/Thermo Fisher Scientific, 4444557) with the following primers: *SCX* (Thermo Fisher Scientific, Hs03054634_g1) and *GAPDH* (Thermo Fisher Scientific, Hs02786624_g1). RT-qPCR was performed to assess activation using PowerUp SYBR Green Master Mix (Applied Biosystems/Thermo Fisher Scientific, A25777) with the following primers (all from Qiagen): *GAPDH* (QT00079247), *COL1A1* (QT00037793), *COL1A2* (QT00072058), and *ACTA2* (QT00088102). Samples were amplified on an ABI 7900HT FAST PCR system (Applied Biosystems/Thermo Fisher Scientific). For analysis, the $2^{-\Delta\Delta Ct}$ quantification method using *GAPDH* for normalization was used. Expression was calculated relative to average mRNA expression levels from control samples.

EdU Click-iT immunofluorescence staining

EdU incorporation into DNA was detected using the Click-iT EdU Alexa Fluor Imaging kit (Invitrogen/Thermo Fisher Scientific, C10640). Fixed primary human FAP^+ Myofibs labeled with EdU were washed in PBS containing 3% BSA and permeabilized in 0.5%

(fibrotic region) shows PDPN (yellow), PDGFRB (purple), and DAPI (blue). Bar = 100 μm. A dashed line marks the border of the fibrotic nodule. (**g**) Enrichment of selected GO terms. VSMC and pericyte are indicated at the top; FB and Myofib are indicated at the bottom. *P*-values were determined by Fisher's exact test. DD, Dupuytren's disease; EC, extracellular; ECM, extracellular matrix; FB, fibroblast; GO, Gene Ontology; Myofib, myofibroblast; SF, Skoog's fascia; UMAP, uniform manifold approximation and projection; VSMC, vascular smooth muscle cell.

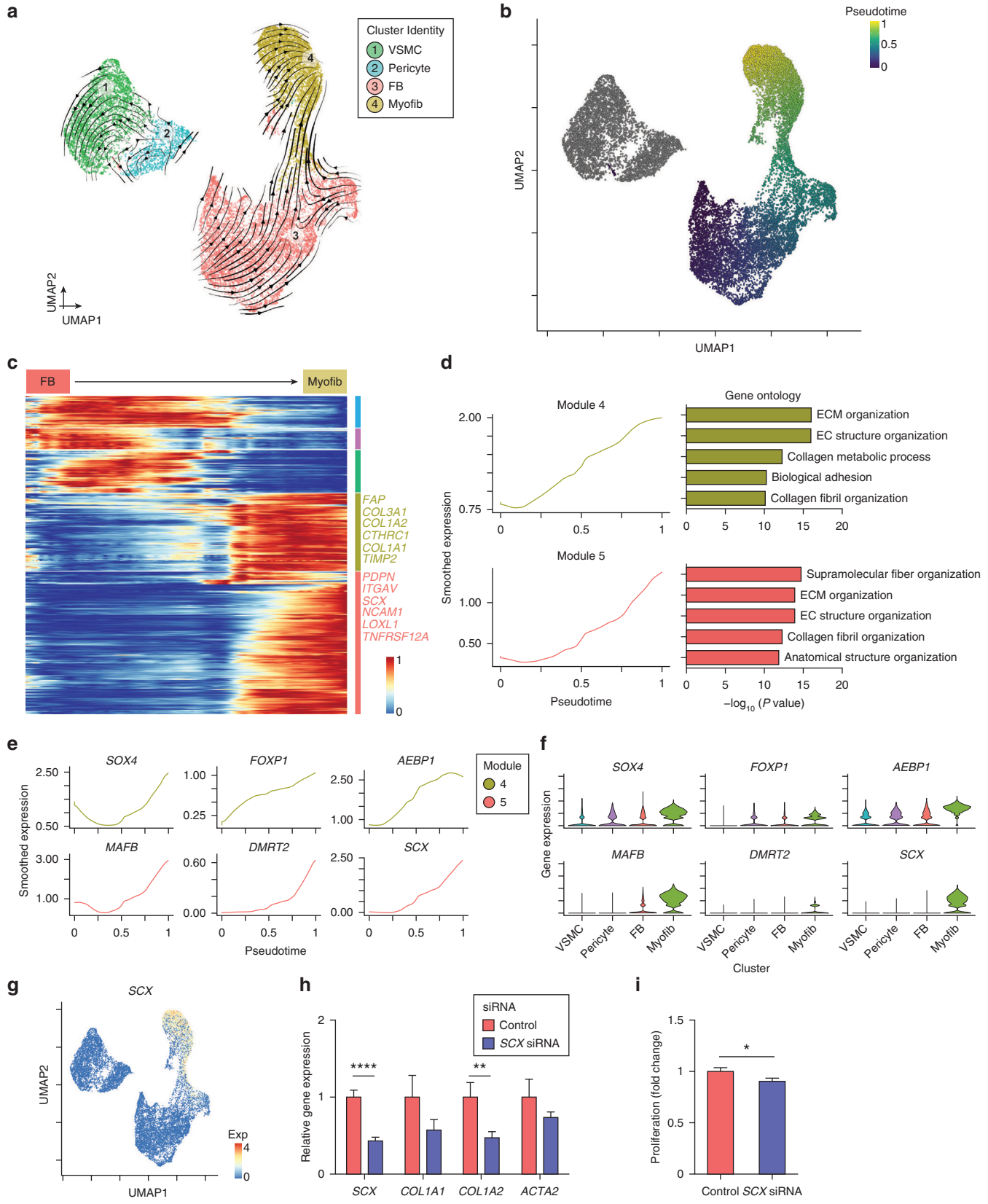

Figure 3. Pathogenic regulation of DD. (**a**) UMAP visualization of RNA velocity stream (black arrows) across mesenchymal clusters. (**b**) UMAP visualization of slingshot pseudotemporal dynamics (purple to yellow) across FB to Myofib mesenchymal subpopulations. (**c**) Heatmap of spline curves fitted to genes differentially expressed along the FB to Myofib pseudotemporal trajectory, grouped by hierarchical clustering (k = 5). Gene coexpression modules (color) and exemplar genes from modules 4 and 5 are labeled (right). (**d**) Spline curve fitted to the averaged expression of all genes in modules 4 and 5 along the pseudotemporal trajectory, with selected enrichment of gene ontology terms (right). *P*-values were determined by Fisher's exact test. (**e**) Spline curves of upregulated transcription factors identified from the Human Transcription Factor database (Lambert et al., 2018) along the pseudotemporal trajectory.

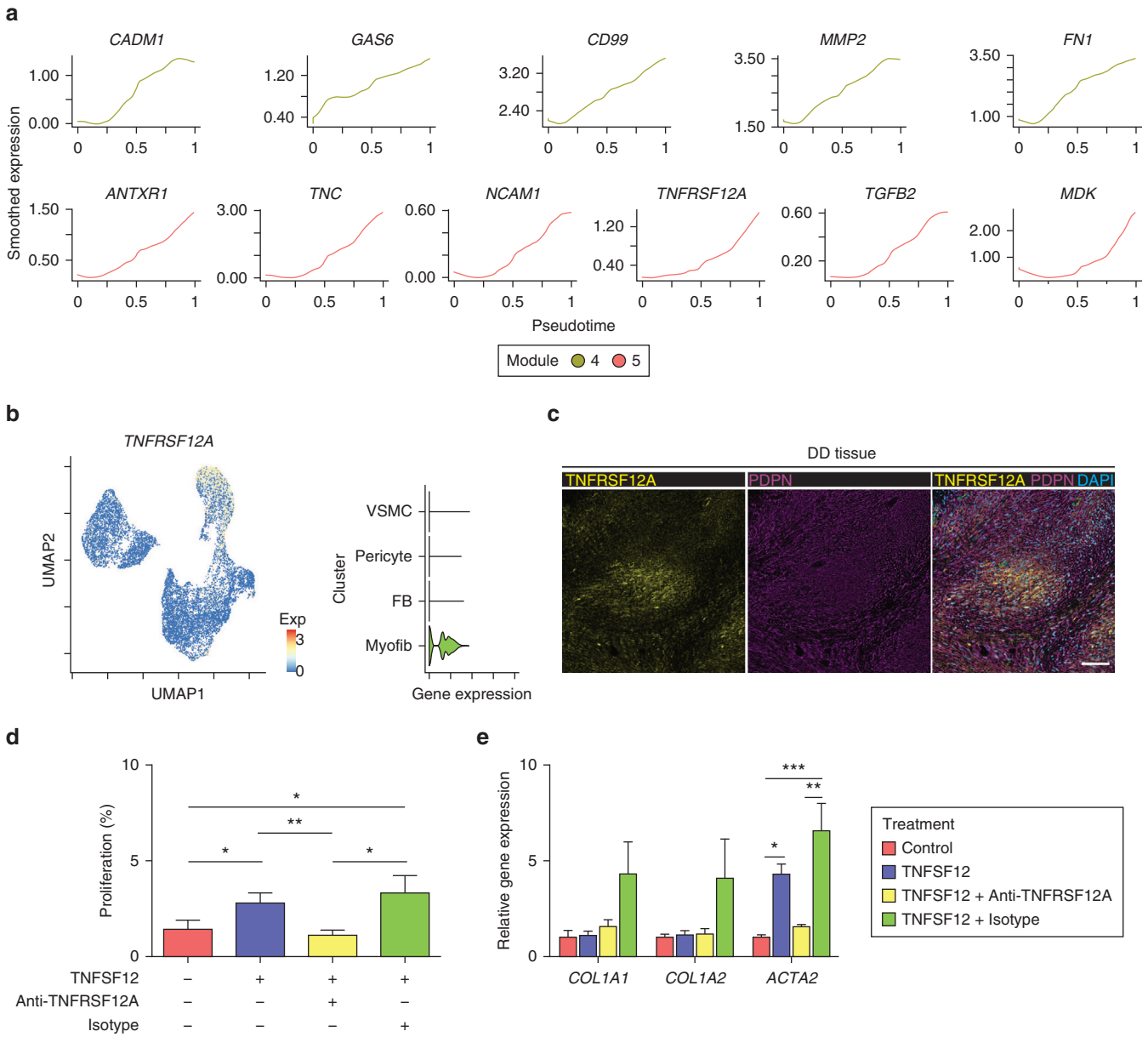

Figure 4. Targeting the pathogenic Myofibs in Dupuytren's disease. (**a**) Spline curves of selected upregulated ligands and receptors identified from CellPhoneDB (Efremova et al., 2020) along the FB to Myofib pseudotemporal trajectory. (**b**) *TNFRSF12A* expression in subsetted mesenchyme dataset (left) and across mesenchymal clusters (right). (**c**) Representative immunofluorescence images of TNFRSF12A (yellow), PDPN (purple), and DAPI (blue) in DD tissue (fibrotic region). Bar = 100 μm. (**d**) Myofib proliferation assay. Data are mean ± SEM. *P*-values were determined by Kruskal–Wallis test and Dunn test. (**e**) Myofibs blockade using anti-TNFRSF12A. *COL1A1*, *COL1A2,* and *ACTA2* were analyzed by qPCR, with expression relative to the mean expression of vehicle-treated Myofibs. Data are mean ± SEM. *P*-values were determined by one-way ANOVA and Tukey test (*COL1A1* and *ACTA2*) or Kruskal–Wallis and Dunn test (*COL1A2*). For **d** and **e**, $*P < 0.05$, $**P < 0.01$, and $***P < 0.001$. DD, Dupuytren's disease; Exp, expression; FB, fibroblast; Myofib, myofibroblast; UMAP, uniform manifold approximation and projection; VSMC; vascular smooth muscle cell.

Triton X-100 (Sigma-Aldrich, St. Louis, MO, T9284) for 20 minutes. The Click-iT solution, containing an azide coupled to an Alexa Fluor 647 fluorophore, was made according to the manufacturer's instructions. Samples were incubated in the EdU cocktail for 30 minutes and rinsed three times in PBS containing 3% BSA. Nuclei were labeled with Hoechst 33342. Images were taken using a Leica DMi8 (Leica, Wetzlar, Germany) and analyzed using Fiji image software (Schindelin et al., 2012).

(**f**) Expression of upregulated transcription factor genes across mesenchymal clusters. (**g**) *SCX* expression in subsetted mesenchyme dataset. (**h**) Gene knockdown in Myofibs using control or *SCX* siRNA. Indicated genes were analyzed by qPCR, with expression relative to the mean expression of control siRNA-treated Myofibs. Data are mean ± SEM. *P*-values were determined by unpaired *t*-test (*SCX*) or Mann–Whitney test (*COL1A1*, *COL1A2*, *ACTA2*). (**i**) Myofib proliferation assay. Data are presented relative to the mean proliferation of control siRNA-treated Myofibs. Data are mean ± SEM. *P*-values were determined by unpaired *t*-test. For **h** and **i**, $*P < 0.05$, $**P < 0.01$, and $****P < 0.0001$. EC, extracellular; ECM, extracellular matrix; Exp, expression; FB, fibroblast; Myofib, myofibroblast; siRNA, small interfering RNA; UMAP, uniform manifold approximation and projection; VSMC, vascular smooth muscle cell.

Immunofluorescence staining

Immunofluorescence staining was completed on formalin-fixed, paraffin-embedded human tissue as previously described (Ramachandran et al., 2019). All primary antibodies were incubated overnight at 4 °C. A full list of primary antibodies and conditions is shown in Supplementary Table S5.

Fluorescently stained sections were imaged using the slide scanner AxioScan.Z1 (Zeiss, Oberkochen, Germany) at ×20 magnification. Images were processed, and scale bars were added using Zen Blue (Zeiss) and Fiji software.

Cell counting and image analysis

Cell counts for Myofib proliferation (EdU^+ Myofibs) in culture were performed manually from multiple high-powered images per sample.

Droplet-based scRNA-seq

Single cells were processed through the Chromium Single Cell Platform using the Chromium Single Cell 3′ Library and Gel Bead Kit, version 2 (10x Genomics, Pleasanton, CA, PN-120237), or version 3 (10x Genomics, PN-1000075) and the Chromium Single Cell A Chip Kit (10x Genomics, PN-120236) or B Chip Kit (10x Genomics, PN-1000074) as per the manufacturer's instructions. Details of the kits used for each sample can be found as part of the Gene Expression Omnibus submission. In brief, single cells were sorted into PBS + 0.1% BSA, washed twice, and counted using a Bio-Rad TC20 (Bio-Rad Laboratories, Hercules, CA). Cells were added to each lane of the ×10 chip and then partitioned into Gel Beads in Emulsion in the Chromium instrument, where cell lysis and barcoded reverse transcription of RNA occurred, followed by amplification, fragmentation, and 5′ adaptor and sample index attachment. Libraries were sequenced on an Illumina HiSeq 4000 (Illumina, San Diego, CA).

Preprocessing scRNA-seq data

We aligned to the GRCh38 reference genome and estimated cell-containing partitions and associated Unique Molecular Identifiers using the Cell Ranger, version 3.1.0, from 10x Genomics. We excluded genes expressed in fewer than three cells in a sample and cells that expressed <200 genes or mitochondrial gene content >10% of the total Unique Molecular Identifier count. We merged all samples into a single dataset before applying the SCTransform function in the Seurat R package, version 3.2.3 (Satija et al., 2015), regressing on the number of counts.

Dimensionality reduction, clustering, and differential expression analysis

We performed unsupervised clustering and differential gene expression analyses in the Seurat R package, version 3.2.3, determining the principal components used by principal components analysis and tuning the resolution parameter accordingly. We conducted differential gene expression analysis using the default Wilcoxon Rank Sum test to assess significance, retaining only genes with a log-fold change of at least 0.5 and expression in at least 25% of cells in the cluster under comparison.

All heatmaps and uniform manifold approximation and projection visualizations, violin plots, and dot plots were produced using Seurat functions in conjunction with the ggplot2, pheatmap, and grid R packages; uniform manifold approximation and projection visualizations were constructed using the same number of principal components as the associated clustering.

To obtain signature scores across curated lists of known marker genes, we used the AddModuleScore function from Seurat.

Inferring cellular dynamics

We performed RNA velocity quantification using the stochastic model from scVelo, version 0.2.1 (Bergen et al., 2020). We first generated unspliced and spliced count matrices per dataset through the run10× option from velocyto, version 0.17.17 (La Manno et al., 2018), before merging through the concatenate function from AnnData, version 0.7.3 (Wolf et al., 2018), and integrating with the Seurat dataset.

To investigate pseudotemporal dynamics, we applied Slingshot, version 1.4 (Street et al., 2018), to the cell populations of interest. Those genes whose expression was changing in a continuous manner across pseudotime were identified by fitting a generalized additive model (gam R package) with a LOESS term for the pseudotime value.

Lists of ligand–receptor pairs and transcription factors were obtained from CellPhoneDB (https://www.cellphonedb.org/) and the Human Transcription Factors database (http://humantfs.ccbr.utoronto.ca/), respectively.

Code availability

R and python scripts enabling the main steps of the analysis are available from the corresponding author on reasonable request.

Data availability statement

Datasets related to this article can be found at https://www.ncbi.nlm.nih.gov/geo/query/acc.cgi?acc=GSE173252, hosted at the Gene Expression Omnibus (Barrett et al., 2013).

ORCIDs

Ross Dobie: http://orcid.org/0000-0001-9516-315X
Chris C. West: http://orcid.org/0000-0002-2323-3232
Beth E.P. Henderson: http://orcid.org/0000-0003-3747-5766
John R. Wilson-Kanamori: http://orcid.org/0000-0002-1372-9912
Laura J. Kitto: http://orcid.org/0000-0002-3923-9292
Jordan R. Portman: http://orcid.org/0000-0003-3020-3725
Mariana Beltran: http://orcid.org/0000-0001-8321-2479
Sadaf Sohrabi: http://orcid.org/0000-0002-1200-3335
Ahsan R. Akram: http://orcid.org/0000-0003-4605-1682
Prakash Ramachandran: http://orcid.org/0000-0001-5996-2413
Li Yenn Yong: http://orcid.org/0000-0002-6838-7841
Dominique Davidson: http://orcid.org/0000-0003-4809-7422
Neil C. Henderson: http://orcid.org/0000-0002-2273-4094

CONFLICT OF INTEREST

The authors state no conflict of interest.

ACKNOWLEDGMENTS

This work was supported by a Scottish Clinical Research Excellence Development Scheme lectureship funded by National Health Service Education Scotland and the Chief Scientist Office (ref: PCL/18/04) to CCW, a research grant from the William Rooney Plastic Surgery and Burns Research Trust (R01/18) to CCW and NCH, a Medical Research Council Precision Medicine Doctoral Training Programme to JP, a Cancer Research UK Clinician Scientist Fellowship to ARA (ref: A24867), a Medical Research Council Clinician Scientist Fellowship (ref: MR/N008340/1) to PR and a Wellcome Trust Senior Research Fellowship in Clinical Science (ref. 219542/Z/19/Z) to NCH. SS was supported by a bursary from the Scar Free Foundation and the British Society for Surgery of the Hand. We thank the patients who donated tissue for this study. We thank S. Johnston, W. Ramsay, and M. Pattison (QMRI Flow Cytometry and Cell Sorting Facility, The University of Edinburgh, United Kingdom) for technical assistance with FACS and flow cytometry.

AUTHOR CONTRIBUTIONS

Conceptualization: RD, CCW, BEPH, NCH; Data Curation: RD, CCW, BEPH, JRW-K; Formal Analysis: RD, CCW, BEPH, JRW-K, NCH; Funding Acquisition: CCW, NCH; Investigation: RD, CCW, BEPH, LJK, DM, JRP, MB, SS, ARA, PR; Project Administration: RD, CCW, BEPH, NCH; Resources: DD, LYY; Software: JRW-K; Supervision: NCH; Validation: RD, CCW, BEPH; Visualization: RD, CCW, BEPH, JRW-K, NCH; Writing - Original Draft Preparation: RD, CCW, BEPH, JRW-K, NCH; Writing - Review and Editing: RD, CCW, BEPH, JRW-K, NCH

SUPPLEMENTARY MATERIAL

Supplementary material is linked to the online version of the paper at www.jidonline.org, and at https://doi.org/10.1016/j.jid.2021.05.030.

REFERENCES

Arpino V, Brock M, Gill SE. The role of TIMPs in regulation of extracellular matrix proteolysis. Matrix Biol 2015;44–46:247–54.

Ascensión AM, Fuertes-Álvarez S, Ibañez-Solé O, Izeta A, Araúzo-Bravo MJ. Human dermal fibroblast subpopulations are conserved across single-cell RNA sequencing studies. J Invest Dermatol 2021;141:1735–44.e35.

Bagchi RA, Roche P, Aroutiounova N, Espira L, Abrenica B, Schweitzer R, et al. The transcription factor scleraxis is a critical regulator of cardiac fibroblast phenotype. BMC Biol 2016;14:21.

Barrett T, Wilhite SE, Ledoux P, Evangelista C, Kim IF, Tomashevsky M, et al. NCBI GEO: archive for functional genomics data sets – update. Nucleic Acids Res 2013;41:D991–5.

Bergen V, Lange M, Peidli S, Wolf FA, Theis FJ. Generalizing RNA velocity to transient cell states through dynamical modeling. Nat Biotechnol 2020;38:1408–14.

Croft AP, Campos J, Jansen K, Turner JD, Marshall J, Attar M, et al. Distinct fibroblast subsets drive inflammation and damage in arthritis. Nature 2019;570:246–51.

Dobie R, Henderson NC. Unravelling fibrosis using single-cell transcriptomics. Curr Opin Pharmacol 2019;49:71–5.

Dobie R, Wilson-Kanamori JR, Henderson BEP, Smith JR, Matchett KP, Portman JR, et al. Single-cell transcriptomics uncovers zonation of function in the mesenchyme during liver fibrosis. Cell Rep 2019;29:1832–47.e8.

Dulauroy S, Di Carlo SE, Langa F, Eberl G, Peduto L. Lineage tracing and genetic ablation of ADAM12(+) perivascular cells identify a major source of profibrotic cells during acute tissue injury. Nat Med 2012;18:1262–70.

Efremova M, Vento-Tormo M, Teichmann SA, Vento-Tormo R. CellPhoneDB: inferring cell–cell communication from combined expression of multi-subunit ligand–receptor complexes. Nat Protoc 2020;15:1484–506.

Espira L, Lamoureux L, Jones SC, Gerard RD, Dixon IM, Czubryt MP. The basic helix-loop-helix transcription factor scleraxis regulates fibroblast collagen synthesis. J Mol Cell Cardiol 2009;47:188–95.

Gomez IG, Roach AM, Nakagawa N, Amatucci A, Johnson BG, Dunn K, et al. TWEAK-Fn14 signaling activates myofibroblasts to drive progression of fibrotic kidney disease. J Am Soc Nephrol 2016;27:3639–52.

Guerrero-Juarez CF, Dedhia PH, Jin S, Ruiz-Vega R, Ma D, Liu Y, et al. Single-cell analysis reveals fibroblast heterogeneity and myeloid-derived adipocyte progenitors in murine skin wounds. Nat Commun 2019;10:650.

He H, Suryawanshi H, Morozov P, Gay-Mimbrera J, Del Duca E, Kim HJ, et al. Single-cell transcriptome analysis of human skin identifies novel fibroblast subpopulation and enrichment of immune subsets in atopic dermatitis. J Allergy Clin Immunol 2020;145:1615–28.

Henderson NC, Arnold TD, Katamura Y, Giacomini MM, Rodriguez JD, McCarty JH, et al. Targeting of αv integrin identifies a core molecular pathway that regulates fibrosis in several organs. Nat Med 2013;19:1617–24.

Henderson NC, Rieder F, Wynn TA. Fibrosis: from mechanisms to medicines. Nature 2020;587:555–66.

Hinz B, Phan SH, Thannickal VJ, Galli A, Bochaton-Piallat ML, Gabbiani G. The myofibroblast: one function, multiple origins. Am J Pathol 2007;170:1807–16.

Jiang D, Correa-Gallegos D, Christ S, Stefanska A, Liu J, Ramesh P, et al. Two succeeding fibroblastic lineages drive dermal development and the transition from regeneration to scarring. Nat Cell Biol 2018;20:422–31.

Kuppe C, Ibrahim MM, Kranz J, Zhang X, Ziegler S, Perales-Patón J, et al. Decoding myofibroblast origins in human kidney fibrosis. Nature 2021;589:281–6.

La Manno G, Soldatov R, Zeisel A, Braun E, Hochgerner H, Petukhov V, et al. RNA velocity of single cells. Nature 2018;560:494–8.

Lambert SA, Jolma A, Campitelli LF, Das PK, Yin Y, Albu M, et al. The human transcription factors [published correction appears in Cell 2018;175:598–9]. Cell 2018;172:650–65.

Layton TB, Williams L, McCann F, Zhang M, Fritzsche M, Colin-York H, et al. Cellular census of human fibrosis defines functionally distinct stromal cell types and states [published correction appears in Nat Commun 2020;11:3275]. Nat Commun 2020;11:2768.

Murray IR, Gonzalez ZN, Baily J, Dobie R, Wallace RJ, Mackinnon AC, et al. αv integrins on mesenchymal cells regulate skeletal and cardiac muscle fibrosis. Nat Commun 2017;8:1118.

Ramachandran P, Dobie R, Wilson-Kanamori JR, Dora EF, Henderson BEP, Luu NT, et al. Resolving the fibrotic niche of human liver cirrhosis at single-cell level. Nature 2019;575:512–8.

Ramírez-Aragón M, Hernández-Sánchez F, Rodríguez-Reyna TS, Buendía-Roldán I, Güitrón-Castillo G, Núñez-Alvarez CA, et al. The transcription factor SCX is a potential serum biomarker of fibrotic diseases. Int J Mol Sci 2020;21:5012.

Satija R, Farrell JA, Gennert D, Schier AF, Regev A. Spatial reconstruction of single-cell gene expression data. Nat Biotechnol 2015;33:495–502.

Schindelin J, Arganda-Carreras I, Frise E, Kaynig V, Longair M, Pietzsch T, et al. Fiji: an open-source platform for biological-image analysis. Nat Methods 2012;9:676–82.

Street K, Risso D, Fletcher RB, Das D, Ngai J, Yosef N, et al. Slingshot: cell lineage and pseudotime inference for single-cell transcriptomics. BMC Genomics 2018;19:477.

Tabib T, Morse C, Wang T, Chen W, Lafyatis R. SFRP2/DPP4 and FMO1/LSP1 define major fibroblast populations in human skin [published correction appears in J Invest Dermatol 2018;138:2086]. J Invest Dermatol 2018;138:802–10.

van Rijssen AL, Ter Linden H, Werker PMN. Five-year results of a randomized clinical trial on treatment in Dupuytren's disease: percutaneous needle fasciotomy versus limited fasciectomy. Plast Reconstr Surg 2012;129:469–77.

Verjee LS, Midwood K, Davidson D, Essex D, Sandison A, Nanchahal J. Myofibroblast distribution in Dupuytren's cords: correlation with digital contracture. J Hand Surg Am 2009;34:1785–94.

Verjee LS, Verhoekx JS, Chan JK, Krausgruber T, Nicolaidou V, Izadi D, et al. Unraveling the signaling pathways promoting fibrosis in Dupuytren's disease reveals TNF as a therapeutic target. Proc Natl Acad Sci USA 2013;110:E928–37.

Vorstandlechner V, Laggner M, Kalinina P, Haslik W, Radtke C, Shaw L, et al. Deciphering the functional heterogeneity of skin fibroblasts using single-cell RNA sequencing. FASEB J 2020;34:3677–92.

Wilburn J, McKenna SP, Perry-Hinsley D, Bayat A. The impact of Dupuytren disease on patient activity and quality of life. J Hand Surg Am 2013;38:1209–14.

Wilhelm A, Shepherd EL, Amatucci A, Munir M, Reynolds G, Humphreys E, et al. Interaction of TWEAK with Fn14 leads to the progression of fibrotic liver disease by directly modulating hepatic stellate cell proliferation. J Pathol 2016;239:109–21.

Wolf FA, Angerer P, Theis FJ. SCANPY: large-scale single-cell gene expression data analysis. Genome Biol 2018;19:15.

Yazdani S, Bansal R, Prakash J. Drug targeting to myofibroblasts: implications for fibrosis and cancer. Adv Drug Deliv Rev 2017;121:101–16.

SUPPLEMENTARY MATERIALS

SUPPLEMENTARY REFERENCES

Efremova M, Vento-Tormo M, Teichmann SA, Vento-Tormo R. CellPhoneDB: inferring cell–cell communication from combined expression of multi-subunit ligand–receptor complexes. Nat Protoc 2020;15:1484–506.

Lambert SA, Jolma A, Campitelli LF, Das PK, Yin Y, Albu M, et al. The human transcription factors [published correction appears in Cell 2018;175: 598–9]. Cell 2018;172:650–65.

Layton TB, Williams L, McCann F, Zhang M, Fritzsche M, Colin-York H, et al. Cellular census of human fibrosis defines functionally distinct stromal cell types and states [published correction appears in Nat Commun 2020;11: 3275]. Nat Commun 2020;11:2768.

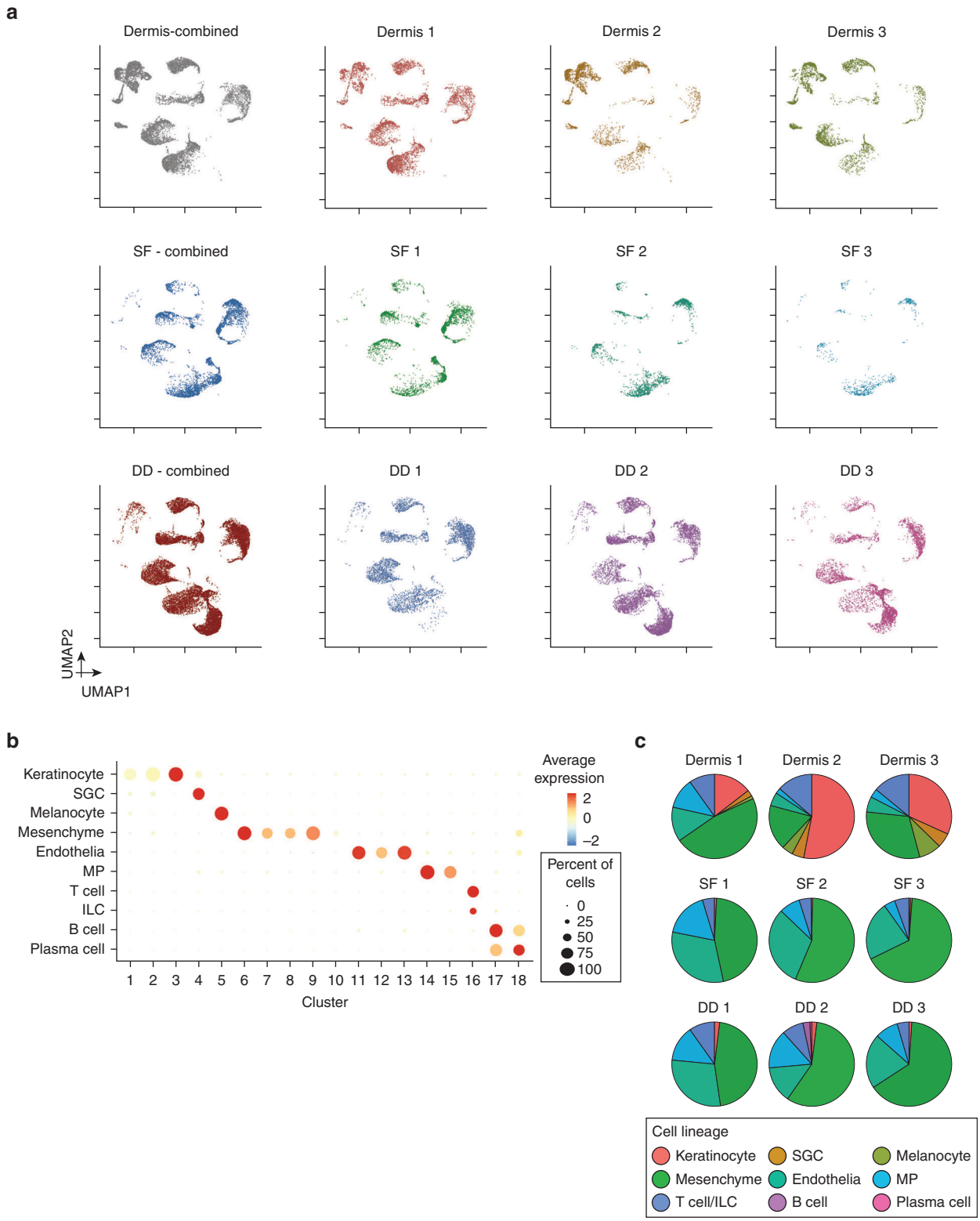

Supplementary Figure S1. Annotation and quality control of human fascia and dermis. This figure is related to Figure 1.(**a**) UMAP visualization of cells per source (leftmost column) and sample. (**b**) Dot plot annotating cell clusters by lineage signature. Circle size indicates cell fraction expressing signature greater than the mean; color indicates mean signature expression (red, high; blue, low). (**c**) Pie charts of the proportion of cell lineage per sample. (**d**) Violin plots of nCount_RNA (top), nFeature_RNA (middle), and percent mitochondrial gene expression (bottom) across cells from dermis (left; n = 3), SF (middle; n = 3), and DD tissue; n = 3) DD, Dupuytren's disease; Exp, expression; ILC, innate lymphoid cell; MP, mononuclear phagocyte; SF, Skoog's fascia; SGC, sweat gland cell; UMAP, uniform manifold approximation and projection.

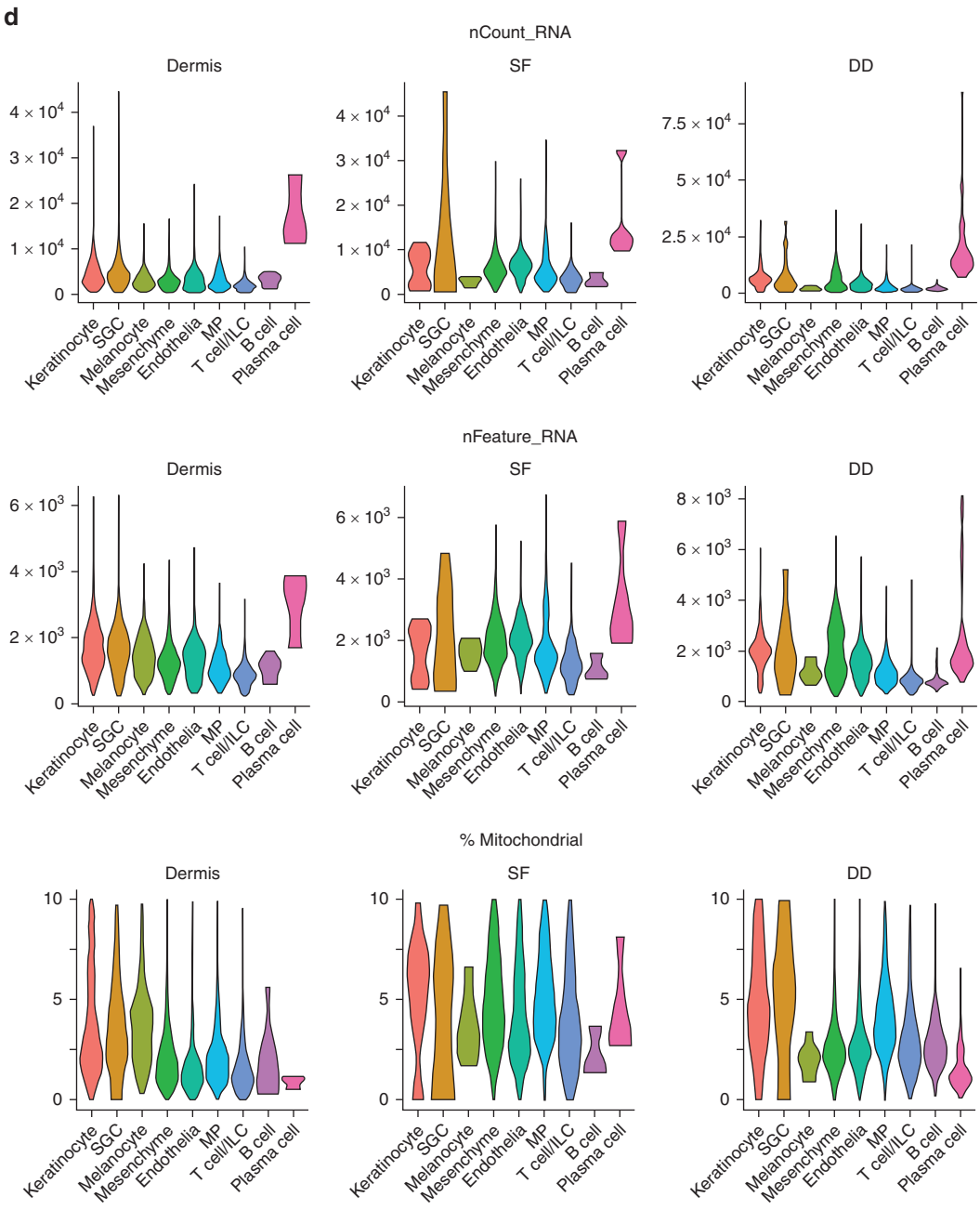

Supplementary Figure S1. Continued.

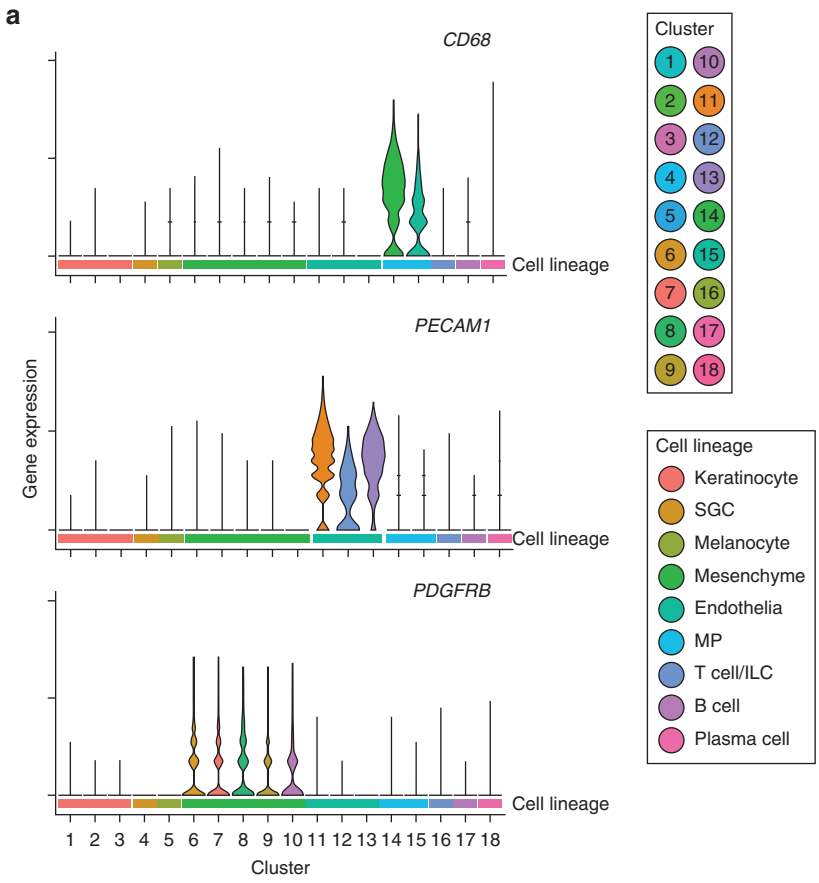

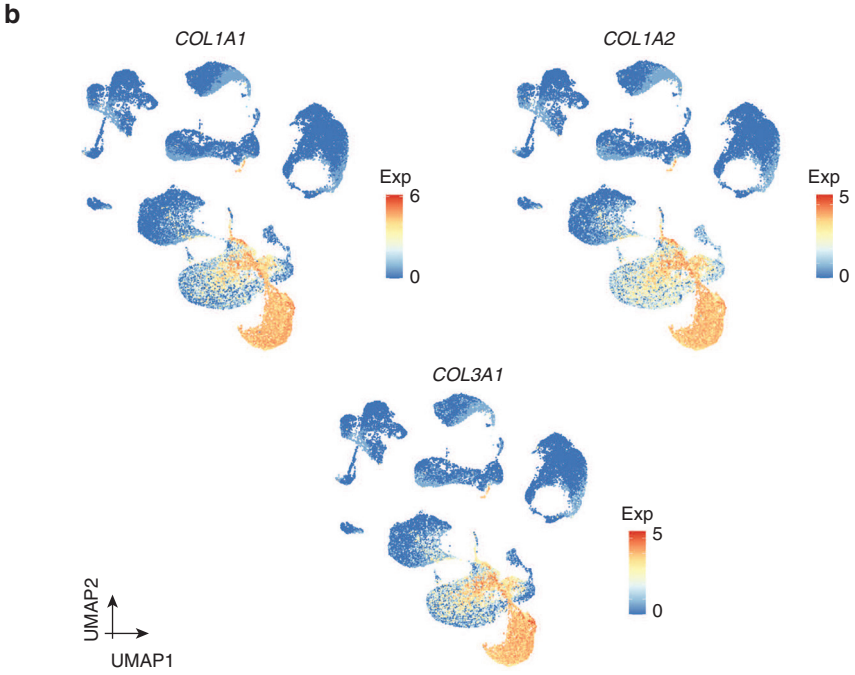

Supplementary Figure S2. Identifying the collagen-expressing cells in DD tissue. This figure is related to Figure 1. (**a**) Expression of selected lineage marker genes across the clusters identified from the dermis (n = 3), SF (n = 3), and DD tissue (n = 3). The lineage is color coded below. (**b**) Expression of fibrillar collagens (*COL1A1*, *COL1A2*, and *COL3A1*) in the full dataset. DD, Dupuytren's disease; Exp, expression; ILC, innate lymphoid cell; MP, mononuclear phagocyte; SF, Skoog's fascia; SGC, sweat gland cell; UMAP, uniform manifold approximation and projection.

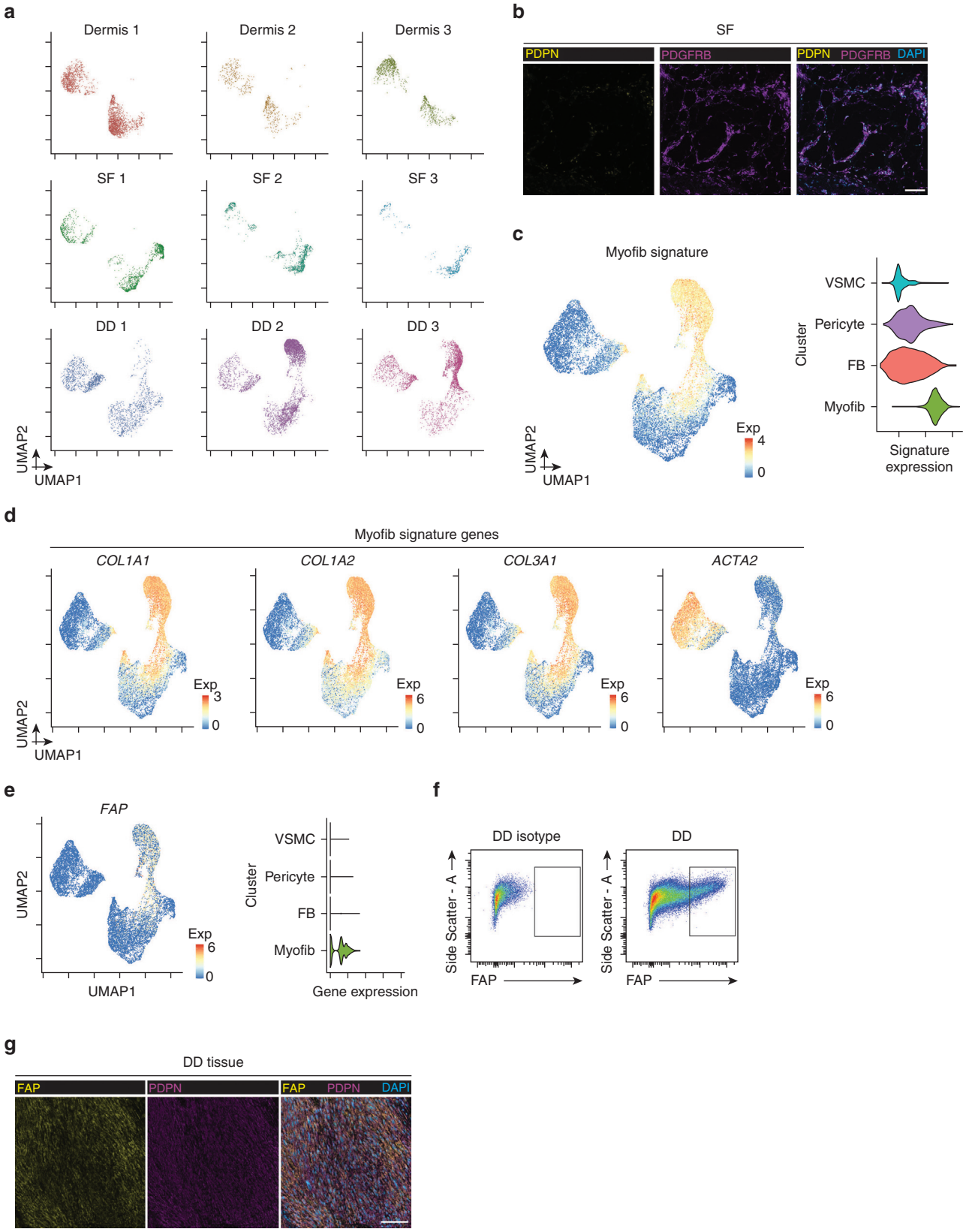

Supplementary Figure S3. Annotation of mesenchymal cells in DD. This figure is related to Figure 2. (**a**) UMAP visualization of cells per sample. (**b**) Representative immunofluorescence images of PDPN (yellow), PDGFRB (purple), and DAPI (blue) in SF. Bar = 100 μm. (**c**) Myofib signature expression in subsetted mesenchyme dataset (left). Expression of Myofib signature across the mesenchymal cells from dermis (n = 3), SF (n = 3), and DD tissue (n = 3) (right). (**d**) Myofib signature genes (*COL1A1*, *COL1A2*, *COL3A1*, and *ACTA2*) expression in subsetted mesenchyme dataset. (**e**) *FAP* expression in subsetted mesenchyme dataset (left) and across mesenchymal clusters (right). (**f**) FACS gating strategy for isolation of Myofibs based on FAP positivity. (**g**) Representative immunofluorescence images of FAP (yellow), PDPN (purple), and DAPI (blue) in DD tissue (fibrotic region). Bar = 100 μm. DD, Dupuytren's disease; Exp, expression; FB, fibroblast; Myofib, myofibroblast; SF, Skoog's fascia; UMAP, uniform manifold approximation and projection; VSMC; vascular smooth muscle cell.

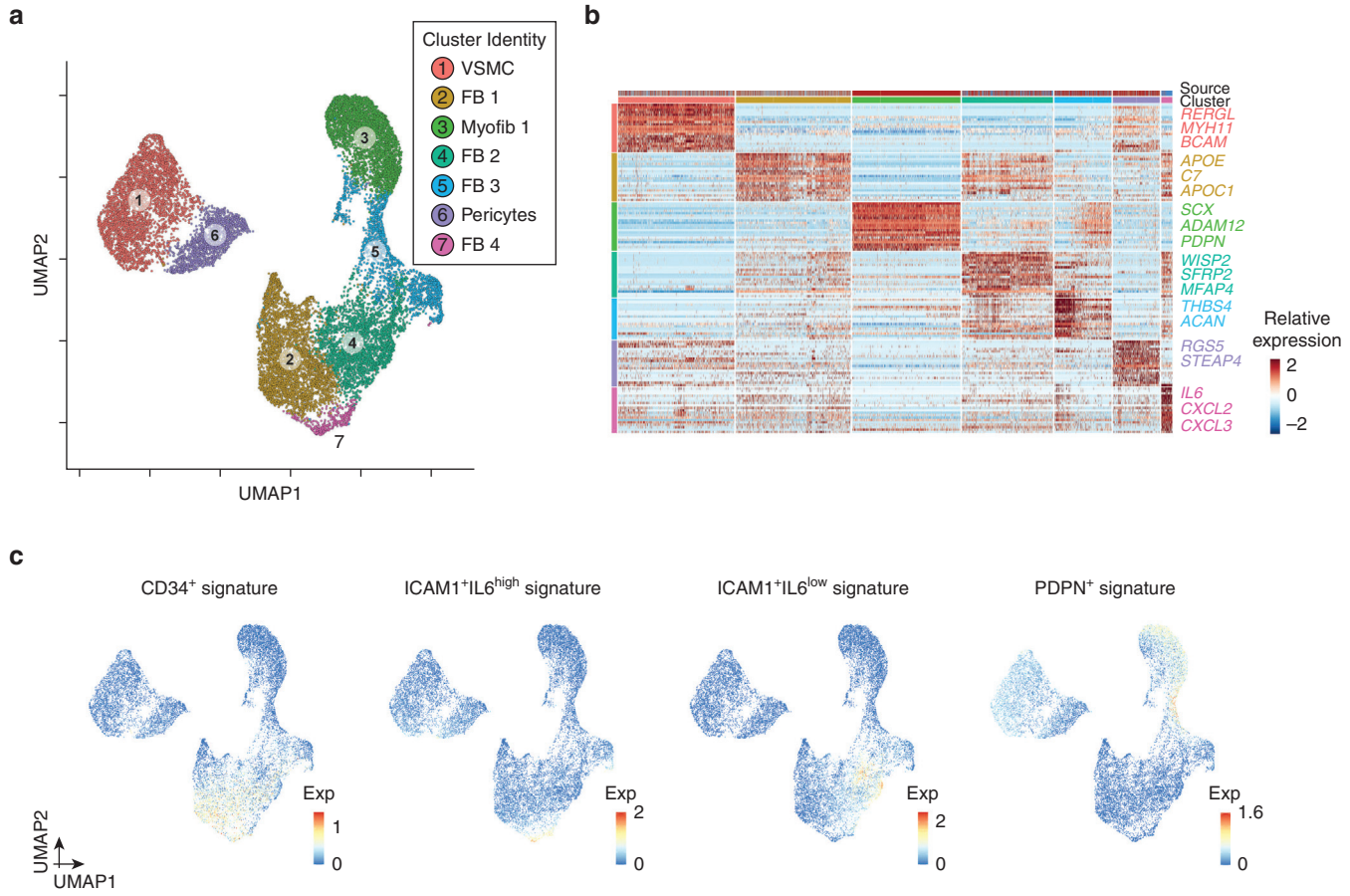

Supplementary Figure S4. Clustering of mesenchymal cells at higher resolution. This figure is related to Figure 2. (**a**) UMAP visualization of the clustering 16,988 mesenchymal cells from dermis (n = 3), SF (n = 3), and DD tissue (n = 3) at higher resolution. (**b**) Heatmap of cluster marker genes (top, color coded by source and cluster), with exemplar genes labeled (right). Columns denote cells; rows denote genes. (**c**) FB subset (CD34^{+}; ICAM1^{+},IL6^{high}; ICAM1^{+},IL6^{low}; PDPN^{+}) signature expression in subsetted mesenchyme dataset. Genes selected for signature analysis were taken from Figure 2d of the study by Layton et al. (2020). DD, Dupuytren's disease Exp, expression; FB, fibroblast; Myofib, myofibroblast; SF, Skoog's fascia; VSMC, vascular smooth muscle cell.

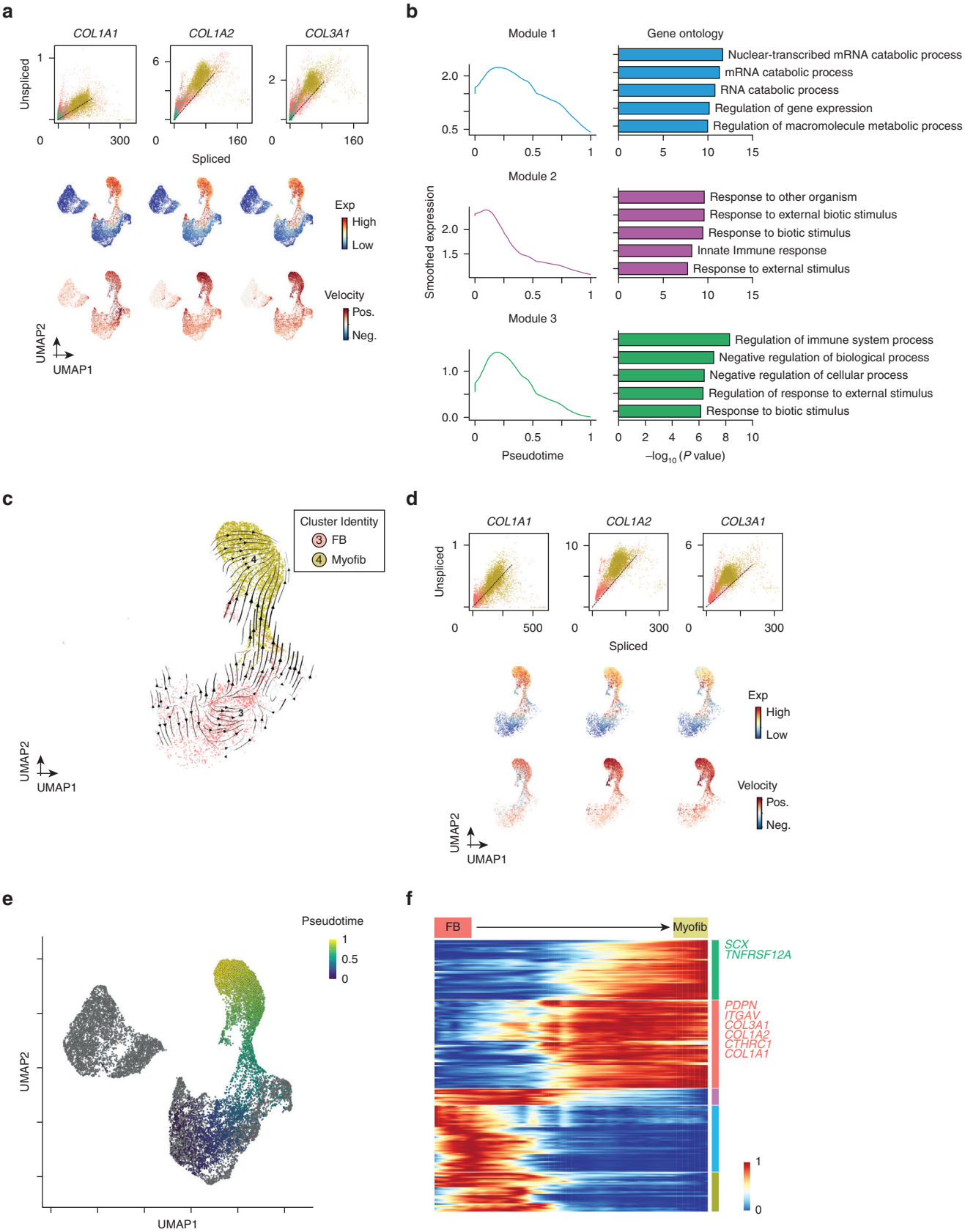

Supplementary Figure S5. Annotating mesenchymal cell trajectory. This figure is related to Figure 3. (**a**) Unspliced–spliced phase portraits (top); 16,988 cells colored and visualized as in Figure 3a; fibrillar collagens (*COL1A1*, *COL1A2*, and *COL3A1*). Cells plotted above or below the steady state (black dashed line) indicate increasing or decreasing expression of genes, respectively. Spliced expression profile for stated genes (middle row; red, high, blue, low). Velocity for stated genes (bottom row); positive (red) indicating expected upregulation and negative (blue) indicating expected downregulation. *COL1A1*, *COL1A2*, and

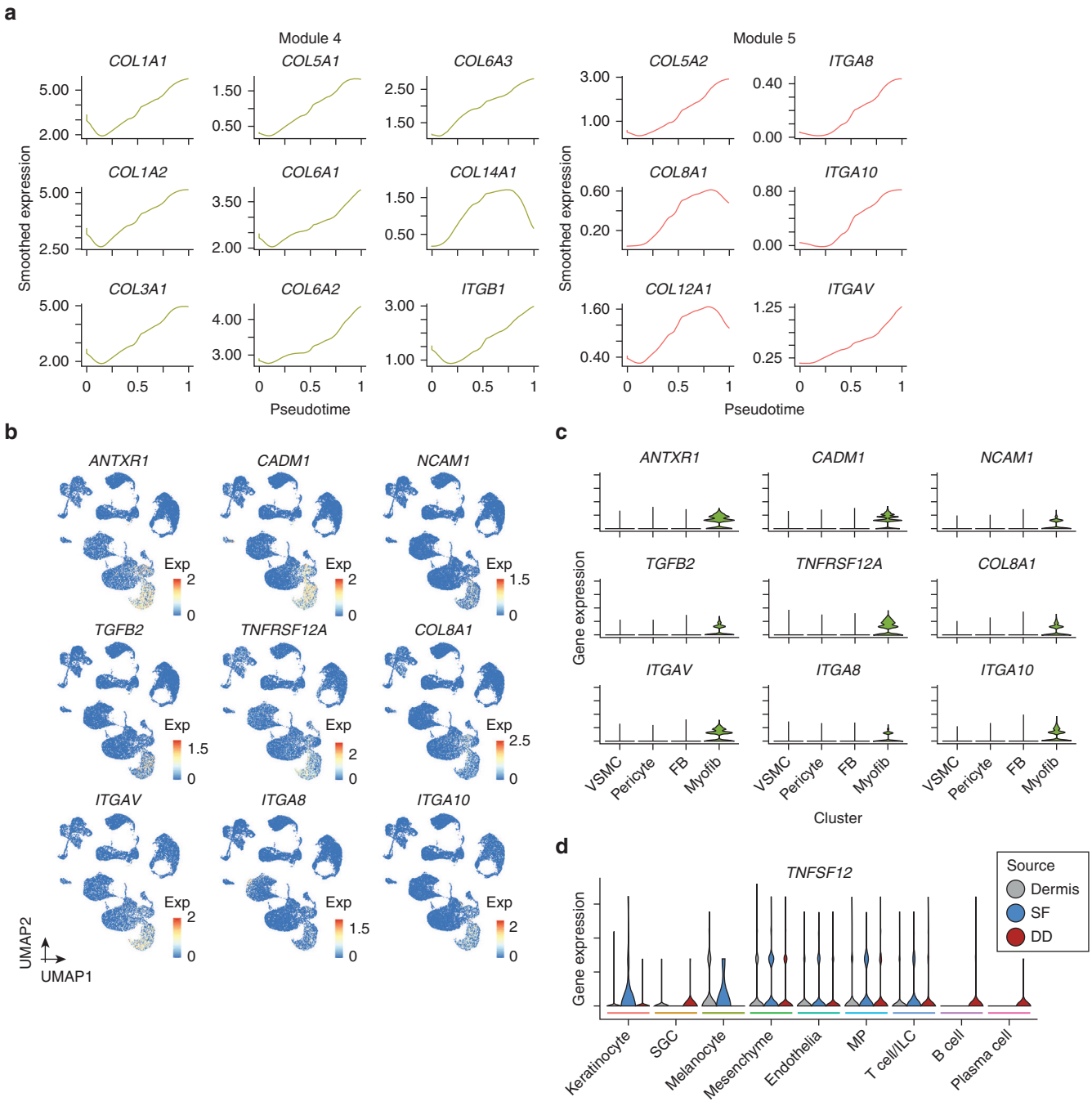

Supplementary Figure S6. Identifying Myofib-specific gene expression in DD. This figure is related to Figure 4. (**a**) Spline curves of upregulated collagen and integrin genes identified from CellPhoneDB (Efremova et al., 2020) along the FB to Myofib pseudotemporal trajectory. (**b**) Expression of selected ligands and receptors in the full dataset, demonstrating mesenchyme specificity. (**c**) Expression of selected ligands and receptors across mesenchymal clusters. (**d**) Expression of *TNFSF12* across the lineages identified from dermis (n = 3), SF (n = 3), and DD tissue (n = 3). The lineage is color coded below. DD, Dupuytren's disease; Exp, expression; FB, fibroblast; ILC, innate lymphoid cell; MP, mononuclear phagocyte; Myofib, myofibroblast; SF, Skoog's fascia; SGC, sweat gland cell; UMAP, uniform manifold approximation and projection; VSMC; vascular smooth muscle cell.

COL3A1 display positive velocity in Myofibs. (**b**) Spline curve fitted to the averaged expression of all genes in modules 1, 2, and 3 from the FB to Myofib pseudotemporal trajectory (see Figure 3c), with selected Gene Ontology enrichment (right). (**c**) UMAP visualization of RNA velocity stream (black arrows) across FB and Myofib clusters containing only cells isolated from DD tissue. (**d**) Unspliced–spliced phase portraits (top); cells colored and visualized as in Supplementary Figure S5c; fibrillar collagens (*COL1A1*, *COL1A2*, and *COL3A1*). Cells plotted above or below the steady state (black dashed line) indicate increasing or decreasing expression of genes, respectively. (**e**) UMAP visualization of Slingshot pseudotemporal dynamics (purple to yellow) across FB to Myofib mesenchymal subpopulations from DD tissue only. (**f**) Heatmap of spline curves fitted to genes differentially expressed along the FB to Myofib pseudotemporal trajectory from DD tissue only, grouped by hierarchical clustering (k = 5). Gene coexpression modules (color) and exemplar genes from modules 1 and 2 are labeled (right). DD, Dupuytren's disease; Exp, expression; FB, fibroblast; Myofib, myofibroblast; Neg, negative; Pos, positive; UMAP, uniform manifold approximation and projection.